Vol 13 No 10, October 2004
1009-1963/2004/13(10)/1657-08

Chinese Physics

© 2004 Chin. Phys. Soc.
and IOP Publishing Ltd

Lattice-Boltzmann simulation of particle-laden flow over a backward-facing step*

Chen Sheng(陈 胜), Shi Bao-Chang(施保昌)†, Liu Zhao-Hui(柳朝晖),
He Zhu(贺 铸), Guo Zhao-Li(郭照立), and Zheng Chu-Guang(郑楚光)

State Key Laboratory of Coal Combustion, Huazhong University of Science and Technology, Wuhan 430074, China

(Received 8 October 2003; revised manuscript received 14 December 2003)

This paper deals with the numerical simulation of gas–solid two-phase flows in an Eulerian–Lagrangian scheme. The particle tracks are calculated using a recently developed exponential Lagrangian scheme, and the approach presently used for the computation of fluid phase is based on a modified Lattice-BGK model. Different from earlier publications, the present study employs a two-way coupling mechanism to handle the interactions between carrier phase and dispersed phase in the model. This new model is applicable to simulating gas–solid two-phase flows. For example, based on the scheme, we have recaptured some phenomena of planar laminar particle-laden flow over a backward-facing step in this research, and found a new interesting phenomenon.

Keywords: lattice-BGK method, particle-laden flow, two-way coupling
PACC: 2852J, 0550, 0270

1. Introduction

The Lattice Boltzmann Method (LBM) and its recent modification, the Lattice-BGK (Bhatnagar–Gross–Krook) model (LBGK), provide an alternative method of simulating fluid flows and modelling complex physics in fluids.[1] In the last decade, the LBM has achieved great success in a variety of fields, ranging form simple laminar flows to turbulent flows,[2,3] flows in porous medium,[4,5] multiphase flows,[6] thermal flows,[7,8] traffic control[9,10] and so on. Nevertheless, there have been few publications[11,12] studying gas–solid two-phase flows that play an increasingly important role in numerous applications. Through using the Eulerian–Lagse studies simulated the motion of particles in uncoupled flow fields which neglected particle–fluid interactions except near boundaries where the shape of boundaries was changed by deposited particles. However, this kind of simplification cannot reflect the realistic phenomena of gas–particle flows even in dilute particle-laden flows[13] which are common in engineering.

Flow separation is a fundamental phenomenon in fluid mechanics. Particle-laden flows are also an interesting phenomenon in the fields ranging from engineering processes to arterial systems. In contrast to the above case, much work,[13,14] which is based on conventional numerical schemes, has been done in the past, predicting the behaviour of laminar particle-laden flow over a backward-facing step. However, none of these studies adopted the LBGK.

In this work we extend the LBGK by employing two-way coupling mechanisms to handle particle–fluid interactions. It provides a new feasible way to simulate gas–solid two phases flows. For example, in this paper we simulate planar laminar particle-laden flows over a backward-facing step. The influence of particle–wall interactions that were overpassed in previous studies is investigated, too. In our study, we not only obtain the same results as those given by previous studies, but also find a new interesting phenomenon.

2. Specification of the problem

The problem domain and boundary conditions are summarized in Fig.1. The channel expands forming the backward-facing geometry with an expansion ratio of 1:2 which is similar to that given by Armaly *et al.*[15] The main channel is $30h$ long, where h is the height of the step. The figure also illustrates the reat-

*Project supported by the National Natural Science Foundation of China (Grant No 60073044), and the State Key Development Programme for Basic Research of China (Grant No G1999022207).
†Corresponding author. E-mail: sbchust@yahoo.com

tachment and separation lengths x_1, x_2 and x_3.

Dimensionless quantities used in this study are defined as

$$\text{Reynolds number} \quad Re = \frac{u_0(2h)}{\nu}, \tag{1}$$

$$\text{Stokes number} \quad Stk = \frac{\rho_p d_p^2 u_0}{18\mu(2h)}, \tag{2}$$

$$\text{Froude number} \quad Fr = \frac{u_0^2}{g(2h)}, \tag{3}$$

$$\text{inlet void fraction} \quad \alpha = V_p/V, \tag{4}$$

where u_0 is the mean inlet channel velocity, μ is the dynamic viscosity, ν is the kinematic viscosity, d_p and ρ_p are the diameter and the density of a particle respectively, V is a unit volume in the fluid field, V_p is the volume occupied by the particles displacement in a unit volume V, and g is gravitational force which acts downwards as shown in Fig.1.

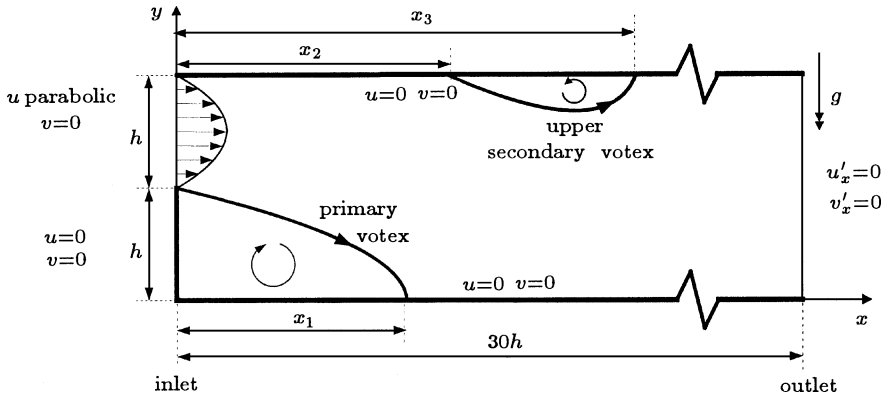


Fig.1. Sketch of backward-facing step, boundary conditions and standing vortices.

3. Governing equations

3.1. LBGK model for incompressible fluid flow

For computation of the fluid phase, an incompressible LBGK model proposed by Guo *et al*[16] is modified because of the presence of a body force $\boldsymbol{F}$ that describes the interactions between the fluid and solid phase

$$g_i(x + c\boldsymbol{e}_i\Delta t, t + \Delta t) - g_i(x,t) = -\frac{1}{\tau}[g_i(x,t) - g_i^{(0)}(x,t)] + f_i\Delta t, \tag{5}$$

where subscript i denotes the velocity direction (i runs from 0 to 8), Δx and Δt are the lattice grid spacing and the time step, respectively. The fluid particle speed, c, is defined as $c = \Delta x/\Delta t$. The dimensionless relaxation time τ is related to the kinematic viscosity as $v = \frac{(2\tau - 1)}{6}\frac{\Delta x^2}{\Delta t}$. In this study τ has a fixed value 0.51. And $g_i(x,t)$ is the density distribution function associated with the fluid particle at node x and time t with a velocity $\boldsymbol{e}_i$; $g_i^{(0)}(x,t)$ is the corresponding local equilibrium distribution function which is determined by

$$g_i^{(0)} = \alpha_i p + s_i(\boldsymbol{u}), \tag{6}$$

where $\alpha_0 = -4\sigma/c^2$, $\alpha_i = \lambda/c^2$ for i=1, 2, 3, 4, and $\alpha_i = \gamma/c^2$ for i=5, 6, 7, 8. Parameters σ, λ, γ satisfy $\lambda + \gamma = \sigma$, $\lambda + 2\gamma = 0.5$. In this paper, we choose σ=5/12, λ=1/3 and γ=1/12. $s_i(\boldsymbol{u})$ is given by

$$s_i(\boldsymbol{u}) = \omega_i\left[3\frac{(\boldsymbol{e}_i\cdot\boldsymbol{u})}{c} + 4.5\frac{(\boldsymbol{e}_i\cdot\boldsymbol{u})^2}{c^2} - 1.5\frac{|\boldsymbol{u}|^2}{c^2}\right] \tag{7}$$

with weight factors ω_0=4/9, ω_i=1/9 for i=1, 2, 3, 4, and ω_i=1/36 for i=5, 6, 7, 8. The macroscopic velocity and pressure of the flow are calculated from the distribution function

$$\boldsymbol{u} = \sum_{i=1}^{8} c\boldsymbol{e}_i g_i, \quad p = \frac{c^2}{4\sigma}\left[\sum_{i=1}^{8} g_i + s_0(\boldsymbol{u})\right]. \tag{8}$$

Finally, the forcing term f_i is given by f_0=0, and $f_i = 3\omega_i\boldsymbol{e}_i\cdot\boldsymbol{F}/c$ for $i = 1,\ldots,8$. Of course, other forms of f_i also can be used.

The Navier–Stokes equation can be derived from Eq.(5):

$$\frac{\partial u}{\partial t} + \nabla\cdot(\boldsymbol{u}\boldsymbol{u}) = -\nabla p + Re^{-1}\nabla^2\boldsymbol{u} + \boldsymbol{F}. \tag{9}$$

3.2. Solid particle motion

Two methods have traditionally been employed for numerically investigating particle-laden flows, the

Eulerian scheme and the Lagrangian scheme. Shirolkar *et al*[17] described the fundamental features of each scheme. It seems probable that the Lagrangian scheme has found more favour with the engineering community in recent years, particularly[18] as the particle phase is solved using the equation of motion for a single particle here. In dilute particle-laden flows the problem is further simplified because various particle–particle interactions, such as collision and coalescence, can be neglected.[17] The present study assumes that the particle is heavier than the surrounding fluid and that the equation of motion can be reduced to a modified Stokes law and the gravitational force[13,14]

$$\frac{\mathrm{d}\boldsymbol{u}_\mathrm{p}}{\mathrm{d}t} = \frac{f}{Stk}(\boldsymbol{u}_f - \boldsymbol{u}_\mathrm{p}) + \frac{1}{Fr}\left(1 - \frac{1}{rho}\right), \qquad (10)$$

where $\boldsymbol{u}_\mathrm{p}$, $\boldsymbol{u}_f$ are velocities of particle and fluid respectively, and rho is the density ratio defined as $rho = \rho_\mathrm{p}/\rho_\mathrm{f}$. The coefficient f describes the influence of the ultra-Stokesian drag[13]

$$f = 1 + 0.15Re_\mathrm{p}^{0.687}. \qquad (11)$$

The term Re_p is the particle Reynolds number and can be calculated by Eq.(12) when $Re_\mathrm{p} < 100$ [14]

$$Re_\mathrm{p} = D_\mathrm{p}|\boldsymbol{u}_\mathrm{f} - \boldsymbol{u}_\mathrm{p}|Re, \qquad (12)$$

where $D_\mathrm{p} = d_\mathrm{p}/(2h)$.

Equation (10) is a stiff equation when $Stk \ll 1$, so we use a recently developed predictor–corrector exponential Lagrangian tracking scheme[13,18] whose global truncation error is $O(\Delta t^2)$. The integration of the equation is achieved by assuming that u_f varies quadratically over the present and previous time step. It can therefore be expressed in the form

$$\boldsymbol{u}_\mathrm{f}(t) = \boldsymbol{u}_\mathrm{f}^n + At + Bt^2, \qquad (13)$$

where $A = \dfrac{\boldsymbol{u}_\mathrm{f}^{n+1} - \boldsymbol{u}_\mathrm{f}^{n-1}}{2\Delta t}$, $B = \dfrac{\boldsymbol{u}_\mathrm{f}^{n+1} - 2\boldsymbol{u}_\mathrm{f}^{n} + \boldsymbol{u}_\mathrm{f}^{n-1}}{2\Delta t^2}$. The superscript n refers to the current time level. The general solutions of the particle velocity and position are expressed as

$$\begin{aligned}\boldsymbol{u}_\mathrm{p}^{n+1} =& \boldsymbol{u}_\mathrm{p}^n \exp\left(\frac{-\Delta t}{\tau_\mathrm{p}}\right) + \boldsymbol{u}_\mathrm{f}^n\left[1 - \exp\left(\frac{-\Delta t}{\tau_\mathrm{p}}\right)\right] \\ &+ A\left\{\Delta t - \tau_\mathrm{p}\left[1 - \exp\left(\frac{-\Delta t}{\tau_\mathrm{p}}\right)\right]\right\} \\ &+ B\left\{\Delta t^2 - 2\tau_\mathrm{p}\Delta t + 2\tau_\mathrm{p}^2\left[1 - \exp\left(\frac{-\Delta t}{\tau_\mathrm{p}}\right)\right]\right\} \\ &+ \tau_\mathrm{p}\left[1 - \exp\left(\frac{-\Delta t}{\tau_\mathrm{p}}\right)\right]G, \qquad (14)\end{aligned}$$

$$\begin{aligned}\boldsymbol{x}_\mathrm{p}^{n+1} =& \boldsymbol{x}_\mathrm{p}^n - \tau_\mathrm{p}(\boldsymbol{u}_\mathrm{f}^n - \boldsymbol{u}_\mathrm{p}^n)\left[1 - \exp\left(\frac{-\Delta t}{\tau_\mathrm{p}}\right)\right] + \boldsymbol{u}_\mathrm{f}^n\Delta t \\ &+ A\left\{\frac{\Delta t^2}{2} - \tau_\mathrm{p}\Delta t + \tau_\mathrm{p}^2\left[1 - \exp\left(\frac{-\Delta t}{\tau_\mathrm{p}}\right)\right]\right\} \\ &+ B\left\{\frac{\Delta t^2}{3} - \tau_\mathrm{p}\Delta t^2 + 2\tau_\mathrm{p}^2\Delta t - 2\tau_\mathrm{p}^3\right. \\ &\left.\times\left[1 - \exp\left(\frac{-\Delta t}{\tau_\mathrm{p}}\right)\right]\right\} \\ &+ \tau_\mathrm{p}\left\{\Delta t + \tau_\mathrm{p}\left[1 - \exp\left(\frac{-\Delta t}{\tau_\mathrm{p}}\right)\right]\right\}G, \qquad (15)\end{aligned}$$

where $\tau_\mathrm{p} = Stk/f$ and $G = (1 - rho^{-1})/Fr$.

4. Boundary conditions and computational methodology

For fluid flow, there are different boundary conditions in this compute plan: at the inlet, a u-parabolic velocity inflow profile is applied; the outflow boundary condition for velocity is $\partial u/\partial x = \partial v/\partial x = 0$; no-slip boundary conditions are prescribed at solid boundaries. Until now, there have been mainly two different kinds of boundary schemes under the above boundary conditions. The first is the extrapolation scheme proposed by Chen *et al.*[22] This scheme is simple and can be extended to include velocity, temperature, and pressure boundary conditions and their derivatives. But unfortunately, the numerical stability of the extrapolation scheme is found to be unsatisfactory.[19] The second is the non-equilibrium extrapolation scheme proposed by Guo *et al*,[19] which has the same advantages as the extrapolation scheme and overcomes the shortcoming of instability. We find that when $Re > 100$ in this problem domain, the numerical results will dissipate if the first boundary scheme is used, although high grid density will improve the numerical stability, while when $Re < 100$, the difference between the two schemes is very small, as shown in Fig.3 (where superscript C denotes extrapolation scheme and G denotes non-equilibrium extrapolation scheme). So we use the non-equilibrium extrapolation scheme[19] to treat all the above boundary conditions.

Regular meshes are uniformly located in the physics plan. There are six different grid densities used in the study: 300×20, 600×40, 690×46, 750×50, 900×60, 1500×100. The first grid density 300×20 is too low to obtain right results. The following two 600×40 and 690×46 are fairly poor compared with the experimental data and other numerical results[13]

at x_2 and x_3 owing to an inadequate grid resolution. And the latter three can give reliable flow field results. The reattachment and separation lengths between 750×50 and 1500×100 are in agreement with the order of 1% (the maximal error appears at x_2), as shown in Figs.4, 7, and 8 (where superscript H denotes higher grid density, i.e. 1500×100, and M denotes medium grid density, i.e. 750×50). However, the latter will consume much more computing time and memory. So in this paper, we mainly show the results acquired under 750×50 grid points. This grid resolution is good enough to obtain reliable flow field results[14] for the present parameters in this study.

The termination condition for the LBGK to compute single-phase flow is that the velocity and pressure residuals are reduced by five orders of magnitude. On a Pentium 4 (2.4G CPU), the time for solutions ranges from 1 to 4 hours, increasing with Reynolds number.

Particles are introduced into the flow at inlets equally spaced along the y direction. Inlet void fraction α is assumed to be uniform across the inlet. The two-phase solutions are not solved directly; instead, the single-phase solutions are initially used and the inlet void fraction is gradually increased, which is as in the study by Barton.[13] Within one time step, flow field and particles evolve one step respectively and particles are injected into the flow N times at an equal time interval. N is determined as follows:

$$N = \frac{6\alpha \boldsymbol{u}_{\mathrm{p}}^{\mathrm{inlet}} \Delta x}{\pi d_{\mathrm{p}}^3}. \tag{16}$$

The term $\boldsymbol{u}_{\mathrm{p}}^{\mathrm{inlet}}$ is the particle inlet velocity, which is assumed to be the same as the surrounding fluid velocity. In order to obtain the body force term $\boldsymbol{F}$ which is derived from the transfer of momentum between phases due to the drag force, we use the method in Ref.[20]

$$F = -rhoV_r \sum_{p=1}^{M} f_p, \tag{17}$$

where V_{r} is the ratio of the volume of one particle to the control volume, M is the number of particles within the control volume and f_p is the drag force acting on a particle. Then $\boldsymbol{F}$ is allocated linearly to grid nodes which surround the control volume. Inelastic collision is used when particles hit against walls; coefficient of restitution e runs from 0 to 0.9.

In the present study, Reynolds number varies from 50 to 700, Stokes number ranges from 1×10^{-5} to 1×10^{-1}, inlet void fraction extends from 1×10^{-6} to 5×10^{-3}, and density ratio rho is 10, similar to that in other numerical studies.[13,14]

5. Results and discussion

5.1. Single-phase flow

The laminar single-phase flow problem has been extensively studied.[13] The behaviour of the flow is briefly summarized as follows. The flow separates at the step and reattaches downstream at position x_1. The position x_1 increases almost linearly. For higher Reynolds numbers the adverse pressure gradient is strong enough to create an upper recirculation region which is illustrated in Fig.1. The upper recirculation region increases in size with increasing Reynolds number, and its core moves downstream. The reattachment and separation positions are summarized in Fig.2, where the experimental data of Armaly *et al*,[15] and the results of Guj and Stella[21] are also shown for justification of using this analysis code. For low Reynolds numbers the present predictions are in good agreement with the experimental data, but for higher Reynolds numbers the numerical predictions start to deviate from the experimental data. The differences are probably caused by three-dimensional effects present in the experiment.[15]

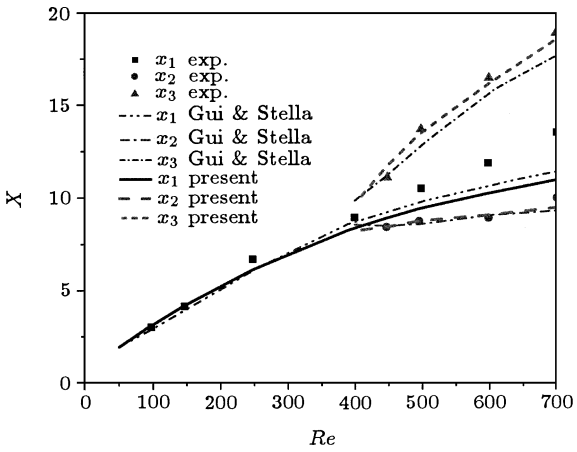


Fig.2. Variation of reattachment and separation lengths with inlet Reynolds number for single-phase flow.

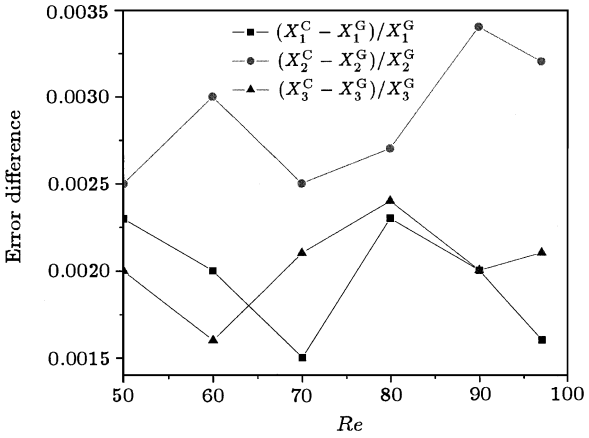


Fig.3. Relative error differences between the extrapolation scheme and the non-equilibrium extrapolation scheme.

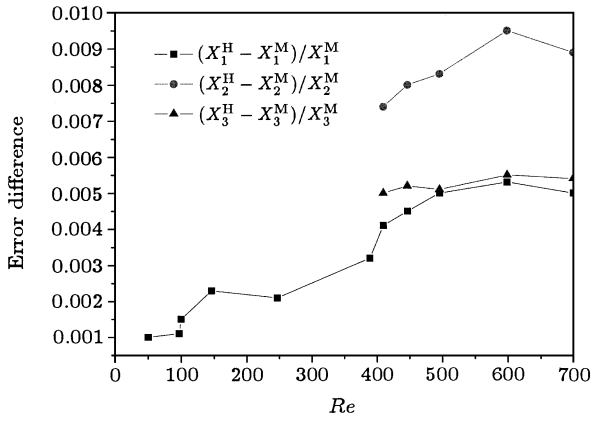


Fig.4. Relative error differences between 750×50 and 1500×100 with Reynolds number for single-phase flow.

5.2. Particle-laden flows

The behaviours of fluid flow and particles depend mainly on Stokes number and inlet void fraction. The behaviours of the various results are considered by assuming one of these parameters to be a constant value and varying the others. Because the emphasis of this study is placed on validating the feasibility of the two-way coupling mechanisms rather than deepening our understanding of particle-laden flow, we do not discuss the relationship of phenomena of the flow to above parameters particularly. For further details see Refs.[13,14].

5.2.1. Variation in Stokes number

As Barton[13] pointed out, low Stokes number particles, which tend to follow the flow, have the effect of reinforcing the freestream of the flow that increases the lower recirculation region. High Stokes number particles are dominated by the effect of gravity that increases downward movement, so they will compress the lower recirculation region and increase the size of the upper recirculation region.

The behaviours of the low and high Stokes number particles are examined for Re=450, 700 and void fraction $\alpha = 3\times10^{-3}$ in Figs.3, 4. The figures show the variation of the reattachment and separation lengths with Stokes numbers. The reattachment and separation lengths for the single-phase flow are also shown in the figures (dashed lines) for comparison with those for the particle-laden flow. The particle-laden flow has either larger or smaller lengths x_1 and x_2 depending on the Stokes number. The particle-laden flow length x_3 is always larger than the single-phase flow length, similar to the results of Barton.[13]

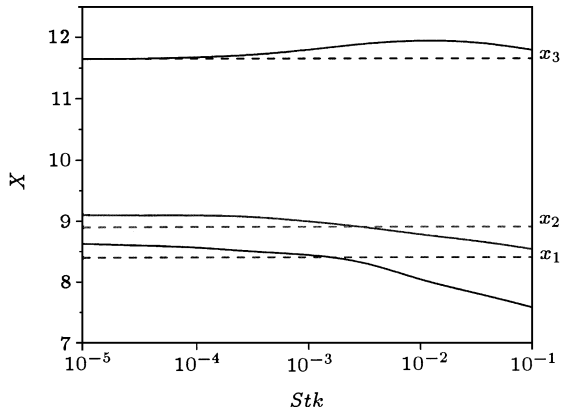


Fig.5. Variation of reattachment and separation lengths with Stokes number for Re=450 and α=3×10^{-3}.

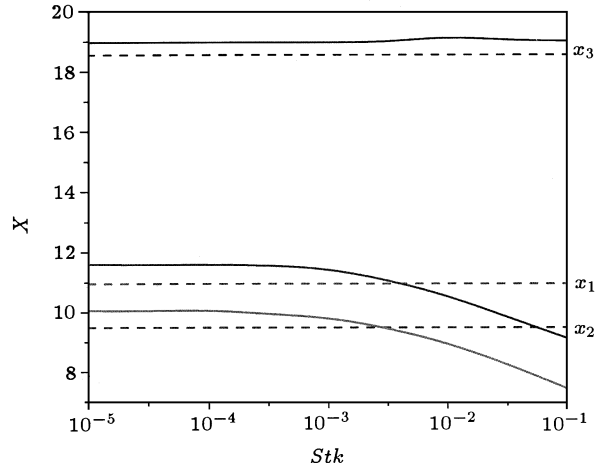


Fig.6. Variation of reattachment and separation lengths with Stokes number for Re=700 and α=3×10^{-3}.

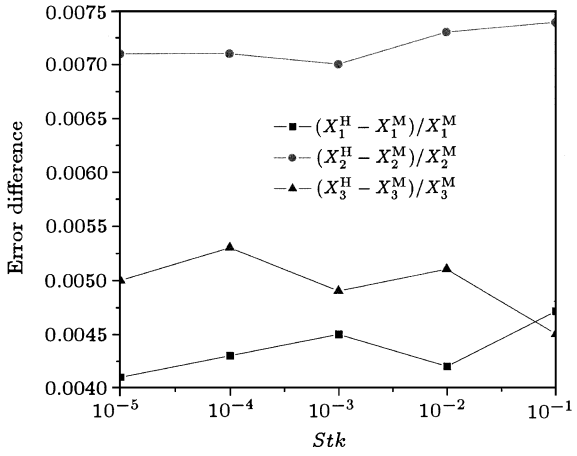


Fig.7. Relative error differences between 750×50 and 1500×100 with Stokes number for Re=450 and α=3×10^{-3}.

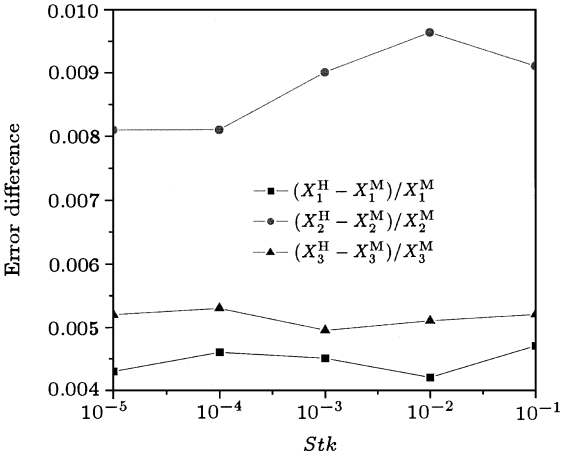


Fig.8. Relative error differences between 750×50 and 1500×100 with Stokes number for Re=700 and α=3×10^{-3}.

5.2.2. Variation in void fraction

We find the same results of two-phase flows as those of single-phase flows up to the void fraction greater than 1×10^{-5}. The differences caused by varying the void fraction are dependent on the Stokes number, as pointed out by Barton.[13] When Stk = 1×10^{-3}, 1×10^{-2} with Re=450 and $\alpha = 3 \times 10^{-3}$, different phenomena appear, similar to those in Ref.[13]: lower Stokes number particles increase the lower recirculation region, and higher Stokes number particles shorten the lower recirculation. A small number of particles enter the lower recirculation region near the lower reattachment; they are transported upstream in the recirculation region almost all the way up to the backward-facing step wall. Barton[13] thought the reason was that $Stk = 1 \times 10^{-2}$ particles were easier to penetrate the lower recirculation region than $Stk = 1 \times 10^{-3}$ particles owing to gravitational force. Figures 9 and 10 show the concentration plots, respectively.

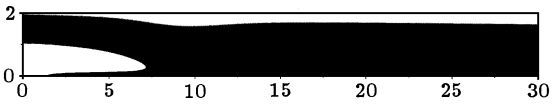


Fig.9. Concentration field of void fraction for Re=450, $Stk = 1 \times 10^{-3}$ and $\alpha = 3 \times 10^{-3}$.

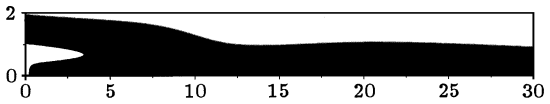


Fig.10. Concentration field of void fraction for Re=450, $Stk = 1 \times 10^{-2}$ and $\alpha = 3 \times 10^{-3}$.

5.2.3. Reynolds number

In this study, we find that low Reynolds number flows vary greatly in behaviour with changes in Stokes number, but because of their small recirculation regions, changes in the lower reattachment length are usually quite small compared with those in the case of moderate Reynolds number (Re=400–500) flows; high Reynolds number flows tend to successfully transport the particles even with high Stokes numbers through the main channel. This is the same as the result in Ref.[13]. We also find an interesting phenomenon: that in low Reynolds number particle-laden flows with high Stokes number particles, when the value of Reynolds number is close to a moderate Reynolds number, there will appear a small secondary upper vortex in the flows and the lower recirculation length is shortened. However, the secondary upper vortex will not appear in single-phase flows that have the same Reynolds numbers. To the best of the authors' knowledge, this phenomenon has not been previously reported. Figure 7 illustrates the process where the secondary upper vortex appears and disappears where Re=389, α=3×10^{-3} and $Stk = 3 \times 10^{-3}$. From the figure we can see that the secondary upper vortex appears at t=139.6 and disappears at t=1236.8. Low recirculation length x_1 becomes smaller during this period and then comes round. Here t is dimensionless time with reference time $t^*=(2h)/u_0$. Figures 12 and 13 show the concentration plots of particles at t=139.6 and 1236.8 respectively. The upper recirculation region of this particle-laden flow is very similar to that of single-phase flow with Re=410. If one of the parameters Reynolds numbers, Stokes number and void fraction is too low, this phenomenon will not appear. In

our study, the critical conditions are: Reynolds number $Re > 290$, Stokes number $Stk > 1 \times 10^{-3}$ and void fraction $\alpha > 1 \times 10^{-3}$. We assume the reason is that particles whose Stokes number are equal to, or greater than, $1{\times}10^{-3}$ are affected by gravity force more or less. The gravity force tends to make the particles deposit along the lower boundary and also within the lower recirculation region. The downward movement of the particles encourages flow downwards along the channel. The downward movement produces the upper vortex and reduces the lower recirculation region size when particles are introduced into the flow inchoately. The effect lasts up to particles distributing almost evenly along the channel.

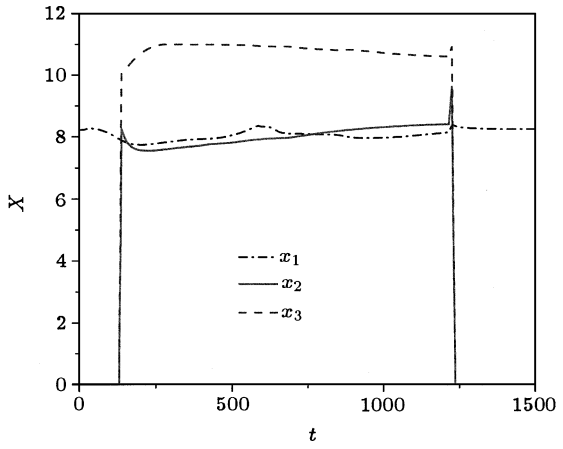


Fig.11. Variation in x_1, x_2 and x_3 with Re=389, α=3×10^{-3} and $Stk = 3 \times 10^{-3}$.

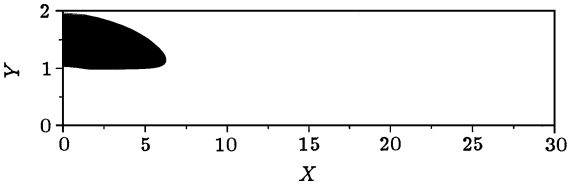


Fig.12. Concentration plot of particles for Re=389, $\alpha = 3 \times 10^{-3}$ and $Stk = 3 \times 10^{-3}$ at t=139.6.

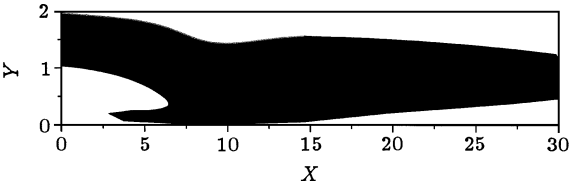


Fig.13. Concentration plot of particles for Re=389, $\alpha = 3 \times 10^{-3}$ and $Stk = 3 \times 10^{-3}$ at t=1236.8.

5.2.4. Particle-wall interactions

In this study, provided that the shape of walls is not changed by deposited particles, we find deposition positions of particles are insensitive to particle–wall interactions when particle-laden flows reach a stable state, i.e. the reattachment and separation lengths x_1, x_2 and x_3 converge. Because when depositional particles approach the lower wall, the x components of velocities of these particles, which are much less than y components of velocities of these particles, are close to zero, their motion of the depositional particles is similar to freefall. For the present geometry that has a large ratio of length to height, deposition positions of particles change very little with different coefficients of restitution.

6. Conclusions

This study is initiated by a lack of two-way coupling mechanisms to handle particle–fluid interactions in previous LBGK simulations. A modified LBGK model is applied to reveal the behaviour of particle-laden flows over a backward-facing step in the Reynolds number range $50 \leq Re \leq 700$, Stokes number range $1{\times}10^{-5} \leq Stk \leq 1 \times 10^{-1}$ and void fraction $1{\times}10^{-6} \leq \alpha \leq 5 \times 10^{-3}$. We conclude that if α is large enough, high Stokes number particles have different effects on flows in contrast with low Stokes number particles because of gravity force, which is the same as the result obtained from the traditional computational fluid dynamics method. And we observe a new phenomenon through this modified LBGK model, which also can be interpreted through the conclusion. In the study, we find in the present geometry that the particle deposition is also insensitive to particle–wall interactions. This new scheme can be modified easily under other conditions, for example three-dimensional simulation.

In the present research, we use two different boundary schemes to handle different boundary conditions. Though the stability of the extrapolation scheme can be improved by adding grid points, it is only suitable for lower Reynolds numbers $Re < 100$ in this computation plan. And the non-equilibrium extrapolation scheme can offer enough accuracy and stability.

There are six different grid resolutions used in the study. For the present parameters in this paper, medium grid density 750×50 is the most effective; lower grid resolution cannot provide accurate results, but higher ones will not be economical in terms of the required computing time. This can be thought of as 'critical grid resolution'. For different parameters such

as Reynolds number or Stokes number, there will be different 'critical grid resolutions'.

In this study, we also use the SIMPLE method to solve fluid phase with the same grid number. Contrasting with the LBGK method, the computing time spent here is about twice the time if the LBGK method is used under the same conditions. Because uniform grids are used in this study, there are a large number of computational points that result in too much time spent in flow field computation. In our program, within a time step, the ratio of times used between flow field and particles is about 1000. So we have a mind to use a nonuniform grid through FDLBE[23] to reduce the total grid number in future.

Acknowledgements

We would like to thank Peng W, Tian Z W and Chen Y M for helpful discussions concerning the modified LBGK model and gas–solid two phases flows.

References

[1] Chen S Y and Doolen Gary D 1998 *Annu. Rev. Fluid Mech.* **30** 329
[2] Benzi R and Succi S 1990 *J. Phys.* A **23** L1
[3] Hou S *et al* 1996*Fields Inst. Comm.* **6** 151
[4] Xu Y S and Xu X Z 2002 *Chin. Phys.* **11** 583
[5] Xu Y S *et al* 2003 *Chin. Phys.* **12** 621
[6] Luo L S 2000 *Phys. Rev.* E **62** 4982
[7] Feng S D *et al* 2001 *Chin. Phys.* **10** 621
[8] He X *et al* 1998 *J. Comp. Phys.* **146** 282
[9] Peng L *et al* 2003 *Acta Phys. Sin.* **52** 1 (in Chinese)
[10] Xue Y *et al* 2004 *Acta Phys. Sin.* **53**1 (in Chinese)
[11] Filippova O and Hanel D 1997 *Comput. & Fluids* **26** 697
[12] Masselot A and Chopard B 1998 *Europhys. Lett.* **42** 259
[13] Barton I E 1996 *Int. J. Numer. Methods Fluids* **22/3** 211
[14] Barton I E 1995 *J. Aerosol Sci.* **26** 887
[15] Armaly B F *et al* 1983*J. Fluid. Mech.* **127** 473
[16] Guo Z L *et al* 2000 *J. Comput. Phys.* **165** 288
[17] Shirolkar J S *et al* 1996 *Prog. Energy Combust. Sci.* **22** 363
[18] Barton I E 2000 *Commun. Numer. Meth. Engng.* **16** 831
[19] Guo Z L *et al* 2002 *Chin. Phys.* **11** 366
[20] Ferrante A and Elghobashi S 2003 *Phys. Fluids* **15** 315
[21] Gui G and Stella F 1988 *Int. J. Numer. Methods Fluids* **8** 405
[22] Chen S *et al* 1996 *Phys. Fluids* **8**2527
[23] Cao *et al* 1997 *Phys. Rev.* E **55** R21